

## Model for dynamical coherence in thin films of self-propelled microorganisms

Igor S. Aranson,<sup>1</sup> Andrey Sokolov,<sup>1,2</sup> John O. Kessler,<sup>3</sup> and Raymond E. Goldstein<sup>3,4,5,6</sup>

<sup>1</sup>Argonne National Laboratory, 9700 South Cass Avenue, Argonne, Illinois 60439, USA

<sup>2</sup>Illinois Institute of Technology, 3101 South Dearborn Street, Chicago, Illinois 60616, USA

<sup>3</sup>Department of Physics, University of Arizona, Tucson, Arizona 85721, USA

<sup>4</sup>Program in Applied Mathematics, University of Arizona, Tucson, Arizona 85721, USA

<sup>5</sup>BIO5 Institute, University of Arizona, Tucson, Arizona 85721, USA

<sup>6</sup>Department of Applied Mathematics and Theoretical Physics, University of Cambridge, Wilberforce Road, Cambridge CB3 0WA, United Kingdom

(Received 7 August 2006; published 2 April 2007)

Concentrated bacterial suspensions spontaneously develop transient spatiotemporal patterns of coherent locomotion whose correlation lengths greatly exceed the size of individual organisms. Continuum models have indicated that a state of uniform swimming order is linearly unstable at finite wavelengths, but have not addressed the nonlinear dynamics of the coherent state, with its biological implications for mixing, transport, and intercellular communication. We investigate a specific model incorporating hydrodynamic interactions in thin-film geometries and show by numerical studies that it displays large scale persistently recurring vortices, as actually observed.

DOI: 10.1103/PhysRevE.75.040901

PACS number(s): 87.16.-b, 05.65.+b, 87.17.Jj

Recent experiments [1–4] have shown that swimming bacteria in concentrated suspensions exhibit an intriguing dynamics that, were it not at such low Reynolds numbers  $Re$ , might be labeled “turbulent.” This new state, dubbed the “Zooming BioNematic” [5], is characterized by transient, recurring swirls and jets with lifetimes of several seconds and correlation lengths ranging from a few tens of microns (in thin films containing either *E. coli* [1] or *B. subtilis* [4]) to several hundred microns (in sessile or pendant drops with *B. subtilis* [3]). Driven entirely by the input of mechanical energy at the smallest scales, through rotation of the helical flagella by motors in the cell wall, these dynamics display a transfer of energy from small scales to large. Such flows in confined geometries are important for fundamental and technological reasons, from understanding coherent motion in groups of interacting objects (flocks, schools, herds [6–8]), to microfluidic devices [9], to highly concentrated populations of bacteria acting as *über*-organisms [10].

Various theoretical models [11–13] have suggested that a state of true long-range order of swimming orientation, suggested by pioneering phenomenology [6,7] and later work [8], is linearly unstable if the long-range interactions between particles are taken into account. The fate of the system beyond that instability has not been well studied within the context of those models. On the other hand, a proposed [3] analogy with sedimenting suspensions, in which transient and recurring vortices and jets are commonly observed, suggested that the structures seen in experiment might arise purely from hydrodynamic interactions. Such interactions appear to underlie as well behavior of sperm cells [14] and *E. coli* [15] near surfaces. Direct numerical simulations [16] of ensembles of self-propelled particles, whose interactions are given solely by the hydrodynamic flow fields they generate, confirm this notion, showing large-scale swirls beyond a critical volume fraction. Yet, while clearly identifying the significance of hydrodynamic interactions, these studies have not yet provided a clear picture of the *mechanisms* of scale selection and the nature of the transition from random mo-

tion at low concentration of swimmers to collective motion at higher concentrations.

Motivated in particular by recent experiments on thin films of bacterial suspensions with controllable density [4], we study here the nonlinear dynamics of a continuum model describing self-propelled particles. The model is formulated in terms of a two-dimensional master equation for the probability density  $P(\mathbf{r}, \phi)$  of finding bacteria at a particular orientational angle  $\phi$  at position  $\mathbf{r}=(x, y)$ , derived from microscopic interaction rules. As we know, purely steric interactions align slender objects [17], a process which has received considerable attention within theoretical biology [18] and physics [19]. Our work also relates to the problem of collective dynamic orientational order in suspensions of biological filaments and motor proteins moving along them [19–21]. The master equation links the scale of individual bacteria to the macroscopic scale of collective motion, described by continuum coarse-grained equations for local bacterial density and orientation. The system is supplemented by the Navier-Stokes equations for the fluid with forcing due to swimming of oriented bacteria. In the nonlinear regime, the model reveals a scale selection mechanism associated with deflection of bacterial swimming by the shear flow, and is in qualitative agreement with experiment [4].

We model the bacteria as polar rods of length  $l$ , diameter  $d_0$ , subject to two rules: (i) bacteria swim at velocity  $v_0$  with respect to the fluid in the direction of their unit orientation vector  $\mathbf{n}=(\cos \phi, \sin \phi)$ ; (ii) in a collision of two bacteria with the angles  $\phi_{1,2}$  the pair swims off in the direction of the average orientation  $\bar{\phi}=(\phi_1+\phi_2)/2$  from a location  $\bar{\mathbf{r}}=(\mathbf{r}_1+\mathbf{r}_2)/2$ , the average of their immediate post-collisional locations. By analogy with the physics of granular matter, we call this a *fully inelastic* collision, and it arises from the quadrupole velocity field of swimmers [16]. It is readily seen in experiment (Fig. 1). Bacteria are also subject to rotational and translational diffusion due to tumbling and small-scale hydrodynamic flows, and are advected by the fluid. The master equation is [19]

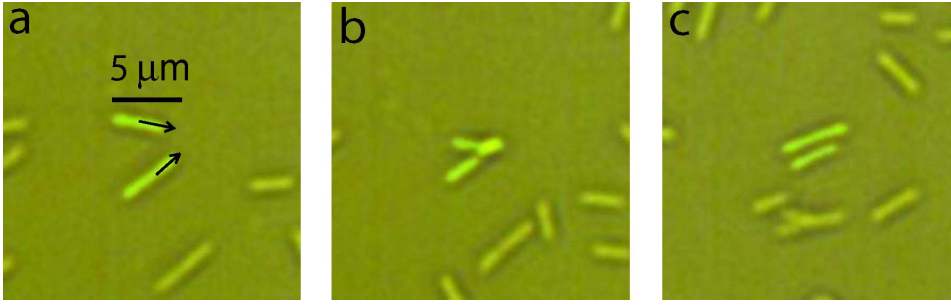


FIG. 1. (Color online) Sequence of experimental images illustrating an “inelastic collision” between swimming *Bacillus subtilis* in a thin film. Colliding bacteria (highlighted) swimming from left to right begin misaligned in (a), reorient during collision (b), and swim off parallel afterwards (c). See Movie 1 in [22].

$$\begin{aligned}
 & \partial_t P + \nabla \cdot [(v_0 \mathbf{n} + \mathbf{v})P] + \frac{1}{2} \Omega \partial_\phi P \\
 &= D_r \partial_\phi^2 P + \partial_i D_{ij} \partial_j P + \int \int d\mathbf{r}_1 d\mathbf{r}_2 \int_{-\pi}^{\pi} d\phi_2 \\
 & \quad \times W(\mathbf{r}_1, \mathbf{r}_2) P(\mathbf{r}_1, \phi_1) P(\mathbf{r}_2, \phi_2) \\
 & \quad \times [\delta(\bar{\mathbf{r}} - \mathbf{r}, \bar{\phi} - \phi) - \delta(\mathbf{r}_2 - \mathbf{r}, \phi_2 - \phi)] - \gamma \left( \mathbf{E} \cdot \mathbf{n} \cdot \frac{\partial P}{\partial \mathbf{n}} \right). \tag{1}
 \end{aligned}$$

The second and third terms on the left-hand side of Eq. (1) account for the hydrodynamic advection of bacteria and their rotation by the flow, whose vorticity is  $\mathbf{\Omega} = (\partial_y v_x - \partial_x v_y) \hat{\mathbf{z}}$ . The first two terms in the right-hand side of Eq. (1) describe angular and translational diffusion of rods with the diffusion tensor  $D_{ij} = [D_{\parallel} n_i n_j + D_{\perp} (\delta_{ij} - n_i n_j)]$ .  $D_{ij}$  are known in polymer physics:  $D_{\parallel} = k_B T_e / \xi_{\parallel}$ ,  $D_{\perp} = k_B T_e / \xi_{\perp}$ , and  $D_r = 4k_B T_e / \xi_r$ , where  $\xi_{\parallel}$ ,  $\xi_{\perp}$ ,  $\xi_r$  are corresponding drag coefficients. For rod-like molecules, they are  $\xi_{\parallel} = 2\pi\eta_s l / \ln(l/d_0)$ ,  $\xi_{\perp} = 2\xi_{\parallel}$ , and  $\xi_r \approx \pi\eta_s l^3 / 3 \ln(l/d_0)$ , where  $\eta_s$  is shear viscosity and  $T_e$  is effective temperature [23]. The effective temperature  $T_e$  is understood here to arise from small-scale hydrodynamic flows and bacterial tumbling, and can exceed considerably the thermodynamic temperature. The last term in Eq. (1) describes the coupling to strain rate tensor  $\mathbf{E}$  ( $E_{xy} = \partial_x v_y + \partial_y v_x$ ) [21,24]. Our further analysis shows that while this term has some quantitative effect, e.g., on the instability threshold, it does not change the qualitative conclusions. Thus for simplicity we set the coupling constant  $\gamma = 0$  and neglect contribution of  $\mathbf{E}$ .

The nonlinear term of Eq. (1) describes short-range binary interactions of rods. The two  $\delta$  functions in the collision integral describe “annihilation” of a particle with the angle  $\phi_1$  and “creation” of particle with the angle  $\bar{\phi}$ . The interaction kernel  $W$  is localized in space, and for the sake of simplicity we neglect the anisotropy of the kernel which is essential for self-organization of microtubules [19]. Kernel anisotropy will generate higher-order terms in the coarse-grained equations which do not affect behavior on a qualitative level [19]. We set  $W = (g/b^2\pi) \exp[-(\mathbf{r}_1 - \mathbf{r}_2)^2/b^2]$  with  $b = l$  and  $g$  the interaction cross section. This form implies that only nearby bacteria interact effectively.

We introduce the coarse-grained density  $\rho(\mathbf{r}) = \int_{-\pi}^{\pi} d\phi P$  and orientation  $\boldsymbol{\tau} = (1/2\pi) \int_{-\pi}^{\pi} d\phi \mathbf{n}(\mathbf{r}) P$ . As shown earlier [19], the *spatially homogeneous* limit of Eq. (1) exhibits on-

set of an oriented state above the critical density  $\rho_c = (D_r/g)/(4/\pi - 1)$ . Near this threshold, Eq. (1) can be simplified significantly by means of a standard bifurcation analysis, yielding a pair of coupled equations for  $\rho$  and  $\boldsymbol{\tau}$ . Also near threshold,  $P$  depends slowly on the variable  $\mathbf{r}$ , so we keep only leading terms in the expansion in spatial gradients of the Fourier expansion of Eq. (1) in  $\phi$ , truncated at second order. With rescalings  $\mathbf{r} \rightarrow \mathbf{r}/l$ ,  $t \rightarrow D_r t$ , and  $\rho \rightarrow g\rho/D_r$ , we obtain [19]

$$\partial_t \rho + \nabla \cdot (\rho \mathbf{v}) = D_0 \nabla^2 \rho - v_0 \pi \nabla \cdot \boldsymbol{\tau}, \tag{2}$$

$$\partial_t \boldsymbol{\tau} + \mathbf{v} \cdot \nabla \boldsymbol{\tau} + \frac{1}{2} \mathbf{\Omega} \times \boldsymbol{\tau} = (\epsilon \rho - 1) \boldsymbol{\tau}$$

$$- A_0 |\boldsymbol{\tau}|^2 \boldsymbol{\tau} + D_1 \nabla^2 \boldsymbol{\tau} + D_2 \nabla \nabla \cdot \boldsymbol{\tau} - \frac{v_0}{4\pi} \nabla \rho. \tag{3}$$

Equation (2) describes advection of the bacteria by hydrodynamic velocity  $\mathbf{v}$  and diffusive spreading with the diffusion coefficient  $D_0$ . Here  $D_1 = (D_{\parallel} + D_{\perp})/2D_r l^2$ ,  $D_2 = (D_{\parallel} - D_{\perp})/2D_r l^2$ . In the rigid rods limit  $D_1 = 5/192$ ,  $D_2 = 1/96$  [19]. For small density  $\rho$  and for the case of pure *thermal* diffusion of particles, the diffusion coefficients obey  $D_0 = (D_{\parallel} + D_{\perp})/2D_r l^2$ . In the present context, this connection is not clear, especially for larger densities due to diffusive-type contributions from the collision integral in Eq. (1). In experiments, there are no significant density fluctuations observed, so we treat  $D_0 \gg D_{1,2}$  as an independent parameter in order to suppress density variations. In Eq. (3) the first term on the right-hand side describes the orientation instability, with  $\epsilon = 0.276$ ,  $A_0 = 2.81$  for fully inelastic particles [19]. Terms proportional to  $v_0$  arise from bacterial swimming with respect to the fluid.

The in-plane fluid velocity  $\mathbf{v}$  obeys the Navier-Stokes equation with forcing due to bacterial swimming

$$\partial_t \mathbf{v} + \mathbf{v} \cdot \nabla \mathbf{v} = \nu \nabla^2 \mathbf{v} - \nabla p - \beta \mathbf{v} + \alpha \boldsymbol{\tau}, \tag{4}$$

with  $\nabla \cdot \mathbf{v} = 0$  by incompressibility. In Eq. (4),  $\nu = v_0/D_r l^2$ , where  $\nu_0$  is the fluid kinematic viscosity,  $p$  is the pressure, and  $\alpha \boldsymbol{\tau}$ , with  $\alpha \sim v_0$ , models the forcing due to bacterial swimming. While our experiments, along with earlier ones [1], are performed in the free-hanging film geometry, the surfactant accumulated on both surfaces of the fluid film play the role of semiflexible walls, resulting in a nontrivial velocity profile across the film. The forcing term in Eq. (4) is formally different from that for the self-propelled particles proposed in Ref. [11], where the force is represented by the

divergence of certain three-dimensional stress tensor  $\sigma_{ij}$ , but integration of that stress tensor over the film's cross section produces a contribution  $\sim \tau$  due to boundary effects. The damping term  $\beta \mathbf{v}$  is generated by the thin film surface elasticity resulting in the partial slip condition for the velocity on the surface of the film.

To eliminate the pressure and satisfy continuity we introduce the stream function  $\varphi$ , with  $v_x = \partial_y \varphi$ ,  $v_y = -\partial_x \varphi$ , and  $\Omega = \nabla^2 \varphi$ . Then Eq. (4) yields

$$\partial_t \Omega + \mathbf{v} \cdot \nabla \Omega = \nu \nabla^2 \Omega - \beta \Omega + \alpha (\partial_y \tau_x - \partial_x \tau_y). \quad (5)$$

Equations (2), (3), and (5) form a closed system. For flows with vanishingly small Reynolds numbers (as we deal with) the advection term  $\mathbf{v} \cdot \nabla \Omega$  can be neglected relative to the viscous dissipation  $\nu \nabla^2 \Omega$ , but we keep it since a similar term is included in Eq. (6). While Re for individual swimming bacteria is exceedingly small, for the collective flows Re can grow significantly. To simplify the analysis we consider the constant density approximation  $\rho = \rho_0$  valid for a large  $D_0$  values. Then Eq. (3) yields

$$\begin{aligned} \partial_t \boldsymbol{\tau} + \mathbf{v} \cdot \nabla \boldsymbol{\tau} + \frac{\boldsymbol{\Omega} \times \boldsymbol{\tau}}{2} = (\epsilon \rho - 1) \boldsymbol{\tau} - A_0 |\boldsymbol{\tau}|^2 \boldsymbol{\tau} + D_1 \nabla^2 \boldsymbol{\tau} \\ + D_2 \nabla \nabla \cdot \boldsymbol{\tau}. \end{aligned} \quad (6)$$

Equations (3), (4), or (5) have a steady-state solution corresponding to a homogeneous stream of bacteria in a certain direction (e.g., along  $x$ ):  $\tau_x = \tau_0 = [(\epsilon \rho - 1)/A_0]^{1/2}$ ,  $\tau_y = v_y = 0$ ,  $\rho = \text{const}$ ,  $v_x = V = \alpha \tau_0 / \beta$ . The most unstable modes in the problem are longitudinal, and we examine stability of this state with perturbations of the form  $(\boldsymbol{\tau}, \Omega) \sim \exp[\lambda t + i k x]$ , where  $\lambda$  is the growth rate and  $k$  is the modulation wave number. Linearization of Eqs. (3) and (5) shows that the equation for  $\tau_x$  splits off, with a growth rate having a strictly negative real part,  $\lambda = -ikV - 2\tau_0^2 - (D_1 + D_2)k^2$ , while  $\tau_y$ ,  $\Omega$  are coupled:

$$\lambda \tau_y = -ikV \tau_y - \frac{1}{2} \Omega \tau_0 - D_1 k^2 \tau_y, \quad (7)$$

$$\lambda \Omega = -ikV \Omega - \nu k^2 \Omega - \beta \Omega - ik \alpha \tau_y. \quad (8)$$

They yield the two growth rates  $\lambda$ :

$$\begin{aligned} \lambda_{1,2} = \frac{1}{2} \left( -(D_1 + \nu)k^2 - \beta - 2ikV \right. \\ \left. \pm \sqrt{[(D_1 + \nu)k^2 - \beta]^2 - 2ik\tau_0 \alpha} \right). \end{aligned} \quad (9)$$

The instability occurs if the product  $\alpha \tau_0$  exceeds a critical value, whose value can be deduced by examining the limit  $k \rightarrow 0$ . An expansion in powers of  $k$  of  $\text{Re}(\lambda)$  yields  $\text{Re}(\lambda) \simeq (\alpha^2 \tau_0^2 / \beta^3 - D_1)k^2 + O(k^4)$ . Clearly, there is a long-wave instability if  $(\alpha \tau_0)^2 > \beta^3 D_1$ . The threshold density for this instability  $\rho_p$  always exceed critical density of the orientation transition  $\rho_c = 1/\epsilon$ . However,  $\rho_p - \rho_c$  is small due to relative smallness of the diffusion  $D_1 \approx 0.026$ . Since  $V = \alpha \tau_0 / \beta$  is the collective steady-state swimming velocity, we can re-express the instability criterion simply as  $V > V_d$ , where  $V_d = \sqrt{\beta D_1}$ . Moreover, since  $\beta \sim \nu / d^2$ , where  $d$  is the film thickness, we

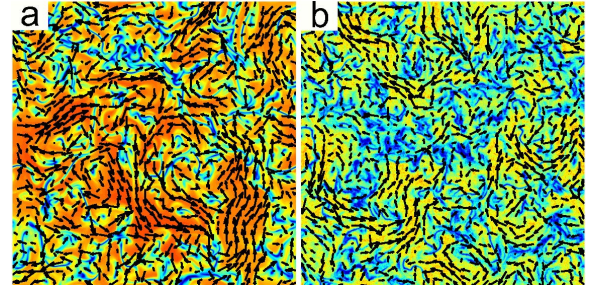


FIG. 2. (Color online) Representative flow patterns obtained by solution of Eqs. (2), (3), (5) for  $\rho_0=3.8$ ,  $D_0=50$ ,  $\nu=3$ ,  $v_0=0.2$ ,  $\alpha=3$ ,  $\beta=0.5$  in the periodic domain of  $200 \times 200$  units. Red color corresponds to maximum of  $|\boldsymbol{\tau}|$ , and blue to  $|\boldsymbol{\tau}|=0$ . Arrows depict the flow velocity  $\mathbf{v}$  field. (a) no noise; (b) noise level  $S=1.2 \times 10^{-5}$ . See also Movie 2 and 3 [22].

find  $V_d = \sqrt{\nu D_1} / d$ . The selected wave number  $k_m$  can be obtained in the limit of large collective swimming speed  $V$ . Expanding Eq. (9) for  $\alpha \tau_0 \gg 1$  we obtain

$$\text{Re}(\lambda) \approx \frac{1}{2} [-(D_1 + \nu)k^2 - \beta + \sqrt{k|\tau_0 \alpha|}] + \dots \quad (10)$$

Then from Eq. (10) one finds [for  $(D_1 + \nu)k^2 \gg \beta$ ]

$$k_m^{3/2} = \sqrt{\tau_0 \alpha} / 4(D_1 + \nu). \quad (11)$$

Since  $\alpha \sim \nu v_0 l / d$ , where again  $l$  is the length of bacteria and  $d$  is the film thickness (here we used expression for the drag force  $F \sim \eta v_0 l$  and included the scaling of orientation  $\tau$  with the film thickness  $d$ ), and  $\tau_0 \sim \sqrt{\rho - \rho_c}$ , where  $\rho_c$  is the critical density of the orientation instability, we obtain  $k_m \sim [v_0 l (\rho - \rho_c)^{1/2} / d \nu^2]^{1/3}$ . Thus the typical length scale of the instability,  $L \sim 1/k_m \sim d^{1/3}$ , increases with the film thickness, in qualitative agreement with the collection of available experiments and numerical computations [16].

We have conducted *numerical studies* of the full system (2), (3), and (5) over a range of densities  $\rho$ , with periodic boundary conditions. A typical flow pattern and distribution of orientation vectors  $|\boldsymbol{\tau}|$  is shown in Fig. 2. Remarkably, over the entire computational domain the correlation between the fields  $\boldsymbol{\tau}$  and  $\mathbf{v}$  is close to zero, in agreement with experiment [4]. However, there is always *local* correlation between  $\boldsymbol{\tau}$  and  $\mathbf{v}$  through Eq. (5).

The following quantities were evaluated: the typical hydrodynamic velocity  $\bar{v} = \sqrt{\langle \mathbf{v}^2 \rangle - \langle \mathbf{v} \rangle^2}$ , and the velocity correlation function  $K(r)$ ,

$$K(r) = \int d\mathbf{r}' \int_0^{2\pi} d\theta \langle \mathbf{v}(\mathbf{r}') \cdot \mathbf{v}(\mathbf{r} + \mathbf{r}') \rangle \quad (12)$$

averaged over the polar angle  $\theta$ . The correlation length  $L$  was extracted from  $K(r)$  by a fit to an exponential decay  $K(r) \sim \exp(-r/L) + \text{const}$ . The results are shown in Fig. 3. The emerging picture of the transition has a strong resemblance to a second order phase transition: the typical velocity  $\bar{v} \sim \sqrt{\rho - \rho_c}$ , and the correlation length diverges at  $\rho \rightarrow \rho_c$ , consistent with the prediction of Eq. (11).

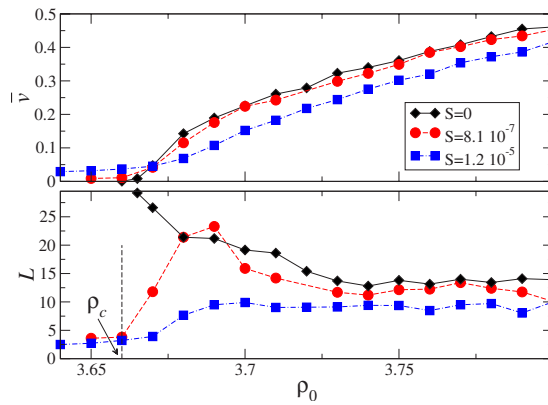


FIG. 3. (Color online) Typical hydrodynamic velocity  $\bar{v}$  (upper panel) and velocity correlation length  $L$  vs density for three different levels of noise  $S$  and for parameters of Fig. 2.

In order to include effect of fluctuation, we added to the orientation equation (3) a random force  $\zeta(x, y, t)$ , with correlation  $\langle \zeta(x, y, t) \zeta^*(x', y', t') \rangle = 2S \delta(x-x') \delta(y-y') \times \delta(t-t')$ , where  $S$  is the noise amplitude. Results for various noise strengths are shown in Fig. 3, where even a relatively small noise ( $S=1.2 \times 10^{-7}$ ) smears the transition and removes the divergence of the correlation length. For strong

enough noise ( $S \sim 10^{-5}$ ), one observes only a gradual increase of the correlation length with the density, in agreement with experiment in thin film [4].

We have proposed a model for the large-scale flows generated by ensembles of swimming bacteria in thin films, and shown that the onset of coherence is attributed to the collective hydrodynamic interaction between individual objects. In identifying a nontrivial mechanism setting the scale of emergent patterns, provides an alternative approach to the description of active hydrodynamic systems [21]. Experimental studies of the dependence of coherent structure scales on lateral boundaries and of the mixing and transport within the collective state are keenly needed. While the equations of motion are derived from simple interaction rules dictated by experiments, additional experimental studies and simple swimmers simulations [16] are required to validate the model (e.g., the values of  $\alpha$  and  $\beta$ ).

We thank Michael Graham, Frank Jülicher, Jacques Prost, Karsten Kruse, Hugues Chate, Jean-Francois Joanny, Eberhard Bodenschatz, and Martin Bees for useful discussions and critical comments. This work was supported by DOE Grant No. DE-AC02-06CH11357, and NSF Grant No. PHY-0551742 (JOK & REG).

- [1] X.-L. Wu and A. Libchaber, *Phys. Rev. Lett.* **84**, 3017 (2000).  
 [2] N. H. Mendelson *et al.*, *J. Bacteriol.* **181**, 600 (1999).  
 [3] C. Dombrowski *et al.*, *Phys. Rev. Lett.* **93**, 098103 (2004); I. Tuval *et al.*, *Proc. Natl. Acad. Sci. U.S.A.* **102**, 2277 (2005).  
 [4] A. Sokolov, I. S. Aranson, R. E. Goldstein, and J. O. Kessler, *Phys. Rev. Lett.* (to be published).  
 [5] L. Cisneros, C. Dombrowski, R. E. Goldstein, and J. O. Kessler, *Phys. Rev. E* **73**, 030901(R) (2006).  
 [6] J. Toner and Y. Tu, *Phys. Rev. Lett.* **75**, 4326 (1995).  
 [7] T. Vicsek *et al.*, *Phys. Rev. Lett.* **75**, 1226 (1995).  
 [8] G. Grégoire and H. Chaté, *Phys. Rev. Lett.* **92**, 025702 (2004).  
 [9] M. J. Kim and K. S. Breuer, *Phys. Fluids* **16**, L78 (2004).  
 [10] *Bacteria as Multicellular Organisms*, edited by J. A. Shapiro and M. Dworkin (Oxford University Press, New York, 1997).  
 [11] R. A. Simha and S. Ramaswamy, *Phys. Rev. Lett.* **89**, 058101 (2002).  
 [12] Y. Hatwalne, S. Ramaswamy, M. Rao, and R. A. Simha, *Phys. Rev. Lett.* **92**, 118101 (2004).  
 [13] R. Voituriez, J. F. Joanny, and J. Prost, *Phys. Rev. Lett.* **96**, 028102 (2006).  
 [14] I. H. Riedel, K. Kruse, and J. Howard, *Science* **309**, 300 (2005).  
 [15] W. R. DiLuzio *et al.*, *Nature (London)* **435**, 1271 (2005).  
 [16] J. P. Hernandez-Ortiz, Ch. G. Stoltz, and M. D. Graham, *Phys. Rev. Lett.* **95**, 204501 (2005).  
 [17] L. Onsager, *Ann. N.Y. Acad. Sci.* **51**, 627 (1949).  
 [18] A. Mogilner and L. Edelstein-Keshet, *J. Math. Biol.* **33**, 619 (1995); *Physica D* **89**, 346 (1996).  
 [19] I. S. Aranson and L. S. Tsimring, *Phys. Rev. E* **71**, 050901(R) (2005); **74**, 031915 (2006).  
 [20] T. B. Liverpool and M. C. Marchetti, *Phys. Rev. Lett.* **90**, 138102 (2003); A. Ahmadi, T. B. Liverpool, and M. C. Marchetti, *Phys. Rev. E* **72**, 060901(R) (2005).  
 [21] K. Kruse *et al.*, *Phys. Rev. Lett.* **92**, 078101 (2004).  
 [22] See EPAPS Document No. E-PLLEE8-75-R17703 for computer animations. A direct link to this document may be found in the online article's HTML reference section. For more information on EPAPS, see <http://www.aip.org/pubservs/epaps.html>.  
 [23] M. Doi and S. F. Edwards, *The Theory of Polymer Dynamics* (Clarendon Press, Oxford, 1988).  
 [24] N. A. Hill and M. A. Bees, *Phys. Fluids* **14**, 2598 (2002).